Journal of Power Sources 195 (2010) 5269–5277

Contents lists available at ScienceDirect

Journal of Power Sources

journal homepage: www.elsevier.com/locate/jpowsour

Effect of manufacturing processes on formability and surface topography of proton exchange membrane fuel cell metallic bipolar plates

Sasawat Mahabunphachai[a,b], Ömer Necati Cora[a], Muammer Koç[a,*]

[a] NSF I/UCR Center for Precision Forming (CPF), Virginia Commonwealth University (VCU), Richmond, VA 23284 USA
[b] National Metal and Materials Technology Center (MTEC), Pathumthani, Thailand

ARTICLE INFO

Article history:
Received 26 January 2010
Received in revised form 5 March 2010
Accepted 8 March 2010
Available online 12 March 2010

Keywords:
Metallic bipolar plate
Microforming
Surface roughness
Contact resistance
PEMFC

ABSTRACT

Metallic bipolar plates in PEM fuel cells offer low-volume, low-mass and low-cost stack fabrication in addition to superior durability when compared to composite bipolar plates, which suffer due to their much higher thickness and less durability. This study aims to address the formability and surface topography issues of metallic bipolar plates fabricated by stamping and hydroforming technologies. Particular emphasis was given to process repeatability, surface topology, and dimensional quality of bipolar plates that would greatly affect the corrosion and contact resistance characteristics. Thin metal sheets of several alloys (i.e., SS304, SS316L, SS430, Ni270, Ti grades 1 and 2) were used in the fabrication experiments. SS304 and SS316L were shown to possess better formability when compared to other alloys that were used in this study, while SS430 and Ti grade 2 demonstrated the worst among all. Channel formability was observed to be greatly affected by the hydroforming pressure, while it does not differ much above certain level of stamping force. The confocal microscopy analyses showed that surface roughness values of the formed samples were altered significantly when compared to the initial flat blanks. In general, increasing hydroforming pressure and stamping force yielded higher surface roughness values at channel peaks. In addition, the surface topography was shown to be influenced mainly by the pressure level rather than the pressure rate in hydroforming process.

© 2010 Elsevier B.V. All rights reserved.

1. Introduction

Fuel cells are considered to be a promising energy conversion technology of the future mainly due to their high efficiency, low noise and minimal emissions particularly for transportation and portable applications. Major automotive companies around the world have already developed and prototyped their first generation fuel cell cars for demonstration purposes. However, these are nowhere near commercialization due to their high cost as well as the lack of supporting infrastructures (e.g., hydrogen refueling station, hydrogen storage and transportation technologies, etc.). Compared to internal combustion engines, fuel cell power is currently 4–10 times more expensive ($200–300 per kW, as compared to $30–50 per kW) [1,2].

Among the various components of the fuel cell, as shown in Fig. 1, the bipolar plates constitutes about 60–80% of the stack weight, 50% of the stack volume and 35–45% of the stack cost [3–7]. The primary roles of bipolar plates are (1) to uniformly distribute reactants (H_2 and O_2) over the membrane electrode assembly through a large array of micro-channels (from 100 μm to 1 mm depth and width) on both sides, (2) to provide a low-resistance electrical interconnect between adjacent cells and the load, and (3) to structurally support the fuel cell stack and to withstand the compressive forces on the stacks. The bipolar plates, therefore, must be thin (200–500 μm), conductive, corrosion resistant, and must have specially designed micro-channels on both sides (for hydrogen and oxygen flow), and at the middle (for cooling fluid) (see Fig. 1). In a proton exchange membrane fuel cell (PEMFC) for a typical passenger car, there are about 400–500 bipolar plates [1,8]. When annual car production volumes are considered to be around 200,000 cars, it becomes quite challenging to develop high speed mass production methods to fabricate bipolar plates of desired quality, consistency and low-cost (<$1 per plate). Therefore, if the weight and cost of the bipolar plates can be reduced, the commercialization of the fuel cell technology would be one step closer. Among the existing types of bipolar plates (e.g., graphite, carbon–polymer composites and metallic plates), metallic plates are leading candidates for the cost-effective and durable PEMFCs. With thin metallic plates (0.5–1 mm), high power stack density can be achieved, while other types cannot get close to this level [9,10]. However, there are two major issues that need to be addressed for metallic bipolar plates prior to full commercialization. The first issue is the poor corrosion resistance of the metallic plates which causes MEA poisoning and performance degradation with time. Several types of metal-based

* Corresponding author. Tel.: +1 804 827 7029.
E-mail address: mkoc@vcu.edu (M. Koç).

0378-7753/$ – see front matter © 2010 Elsevier B.V. All rights reserved.
doi:10.1016/j.jpowsour.2010.03.018

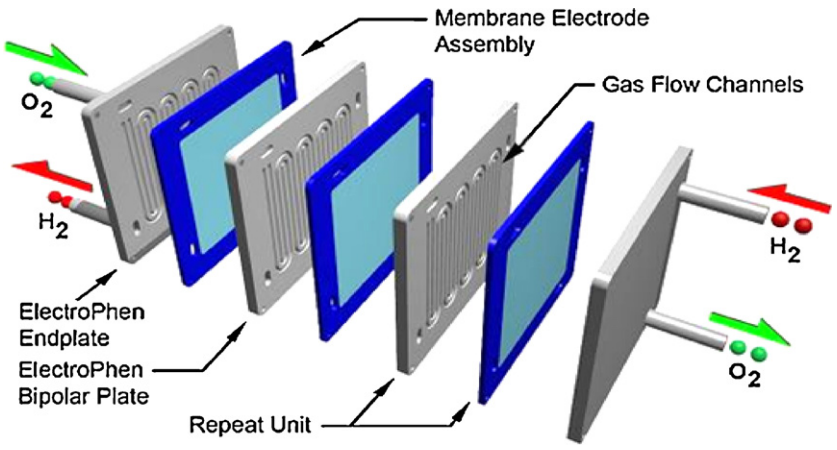

Fig. 1. A typical proton exchange membrane fuel cell (PEMFC) assembly [19].

Table 1
Material properties.

Material	Condition/temper	Mechanical properties		
		Yield strength	Tensile strength	% Elong. in 2 in.
SS304	Cold rolled	31.2 KSI	73.2 KSI	70
SS316L	Annealed	45.1 KSI	100.4 KSI	74
SS430	Cold rolled	N/A	N/A	N/A
Ni270	Cold rolled	N/A	N/A	N/A
Ti Gr. 1	Annealed	27.2 KSI	47.1 KSI	31.4
Ti Gr. 1	Cold rolled	N/A	N/A	N/A

sheet alloys (e.g., SS-, Ni-, Ti-based sheets), with or without coating [5,8,11–13] are being researched in order to meet the minimum requirement of the corrosion resistance (i.e., 1 $\mu A\,cm^{-2}$, Department of Energy Goal by 2010). The second issue is the lack of manufacturing processes that offer high speed, low-cost, high precision and robust fabrication of the thin metallic bipolar plates [14–18]. Repeatability of production process and formed parts is very critical as small variations on the bipolar plate dimensions and surface quality would greatly affect their contact resistance and fuel cell performance.

While machined metallic bipolar plates could meet the high precision and low variation requirements with the latest cutting technologies, this method is far from being cost competitive; and therefore, inappropriate for mass production. On the other hand, metal forming processes, such as stamping, hydroforming, and rolling are well-known for their high productivity rates. In a previous study by the authors, hydroforming process was demonstrated for making arrays of micro-channels on thin stainless steel sheet and the results confirmed the process repeatability as well as controllability [20]. In this study, stamping process is evaluated for its validity as an alternative method for producing the metallic bipolar plates. In addition, the stamping process is compared to the hydroforming process in terms of process capability and repeatability, plate dimensional variations, maximum achievable aspect ratio of the micro-channels, and surface topologies of the fabricated plates.

In the next section, material specifications and experimental setups for both stamping and hydroforming processes are discussed. The experimental results are then analyzed and discussed in section three in terms of their formability and surface quality of the formed bipolar plates. Finally, in section four, a summary of findings and conclusions are presented.

2. Experimental conditions and setup

2.1. Material specifications

Six different metallic sheet alloys were used in this study, all with an initial thickness of 0.051 mm. The mechanical properties and the chemical compositions of these alloys are presented in Tables 1 and 2 as provided by the supplier (Hamilton Precision Metals, Inc., Pennsylvania, USA). The specimens were prepared from the incoming rolls of these alloys into a size of 70 mm × 70 mm, and 152 mm × 152 mm for stamping and hydroforming processes, respectively.

2.2. Experimental setup

A die set was developed in this study to perform both stamping and hydroforming as shown in Fig. 2a. The die set is composed of two die insert holders, one male and one female, and an attachment

Table 2
Chemical compositions.

Material	Chemical composition (wt.%)																
	C	Co	Cr	Cu	Fe	H	Mg	Mn	Mo	N	Ni	O	P	S	Si	Sn	Ti
SS304	<0.08		18–20		Bal.			<2			8–10.5		<0.045	<0.03	<1		
SS316L	0.016		16.25	0.43	Bal.			1.44	2.03	0.04	10.06		0.032	0.001	0.48		
SS430	0.04		16.65		Bal.			0.45			0.14		0.021	0.002	0.41		
Ni270	0.0024	< 0.001	<0.001	<0.001	<0.001		<0.001	<0.001			Bal.			0.0003	<0.001	<0.001	
Ti Gr. 1	0.1				0.03	0.001				0.01		0.05					Bal.
Ti Gr. 1	0.013				0.06	0.0012				0.005		0.14					Bal.

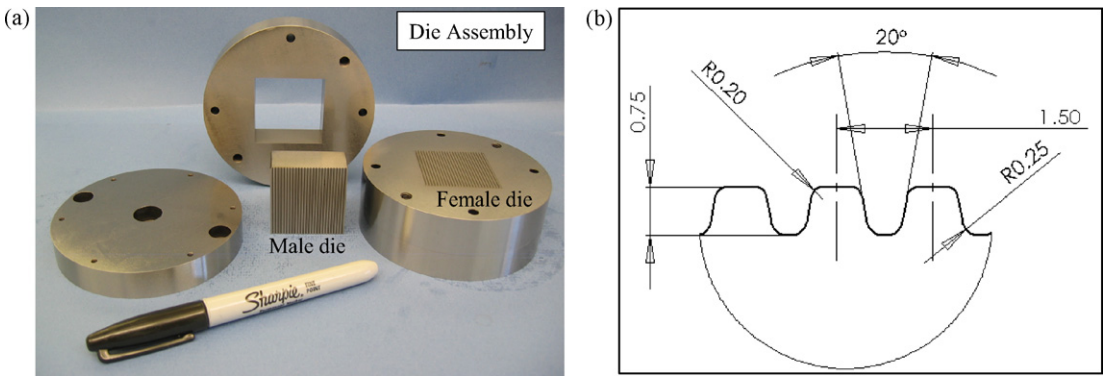

Fig. 2. (a) Die set for stamping and hydroforming, and (b) geometries of micro-channel on the female die.

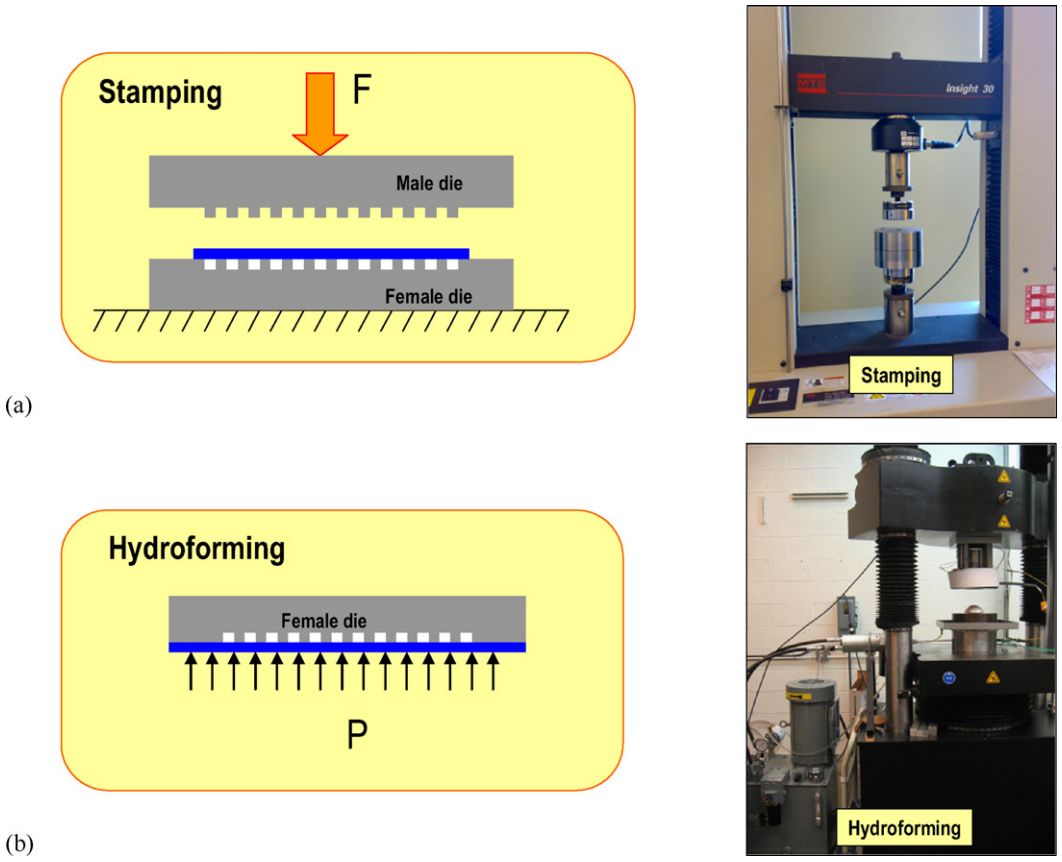

Fig. 3. Setup for (a) stamping, and (b) hydroforming processes.

plate for assembly purposes. Male and female inserts, each with an array of 26 parallel micro-channels, were used for the stamping operation. In hydroforming process, only the female insert was needed as the sheet blanks were formed into the micro-channels by a pressurized fluid media. The selected micro-channel size used in this study is 0.75 mm in channel width, height, and the land area. Fig. 2b depicts a detailed geometry of the insert. The assembly of the die set for both stamping and hydroforming processes on

Table 3
Experimental cases.

Material	Mfg. processes	Speed/rate	Force or pressure
SS304	Stamping	0.1 mm s^{-1}, 1 mm s^{-1}	100 kN, 200 kN, 300 kN
	Hydroforming	0.1 MPa s^{-1}, 1 MPa s^{-1}, 10 MPa s^{-1}	20 MPa, 40 MPa, 60 MPa
SS316L	Stamping	1 mm s^{-1}	100 kN, 200 kN, 300 kN
	Hydroforming	0.1 mm s^{-1}	20 MPa, 40 MPa, 60 MPa
SS430	Stamping	1 mm s^{-1}	200 kN, 400 kN
Ni270	Stamping	1 mm s^{-1}	200 kN, 400 kN
Ti Gr. 1	Stamping	1 mm s^{-1}	200 kN, 400 kN
Ti Gr. 1	Stamping	1 mm s^{-1}	200 kN, 400 kN

the Instron and MTS materials testing systems are shown in Fig. 3. The Instron Satec 5596 machine was used to supply the stamping force and control the stamping speed, while it was used to supply the clamping force during the hydroforming process. The clamping force was set to be 1300 kN and 1500 kN for SS304 and SS316L specimens, respectively.

2.3. Process conditions and measurement setup

In order to assess the capability and repeatability of the stamping and hydroforming processes for fabrication of the metallic bipolar plates, a series of experiments were conducted as summarized in Table 3. For each case, three replications were conducted in order to study the process repeatability and variations. In order to detect the dimensional variations and compare the process capability of the stamping and hydroforming processes, a laser sensor (Keyence LK-G37) that has high repeatability of 0.05 μm was used to measure the micro-channel profiles. The effect of the forming process on the surface topography was analyzed using a confocal microscope (μsurf explorer, Nanofocus Inc., Glen Allen, VA, USA).

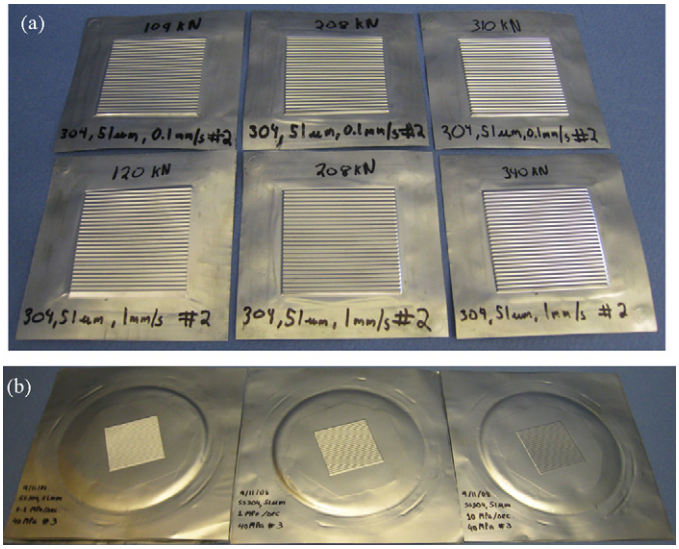

Fig. 4. Samples of (a) stamped, and (b) hydroformed specimens.

3. Results and discussion

3.1. Repeatability of stamping and hydroforming processes

Examples of the hydroformed and stamped bipolar plates are shown in Fig. 4. Typical profile measurements obtained from the laser sensor are shown in Fig. 5. The channel height values as measured using the laser sensor were plotted in Fig. 6 for SS304. Fig. 6a shows the in-plate variations which were captured by measuring the micro-channel profiles at three different locations (i.e., left, middle and right) on the same bipolar plate (BPP). The results indicate that maximum in-plate variations are 4.1% and 1.3% for the stamped and hydroformed BPPs, respectively. On the other

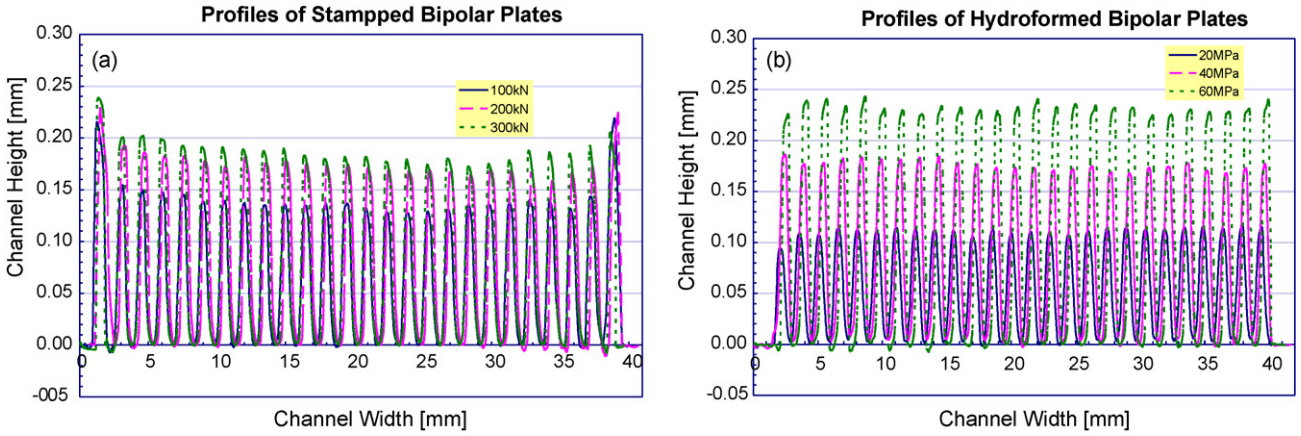

Fig. 5. Laser measurement profiles of (a) stamped, and (b) hydroformed specimens.

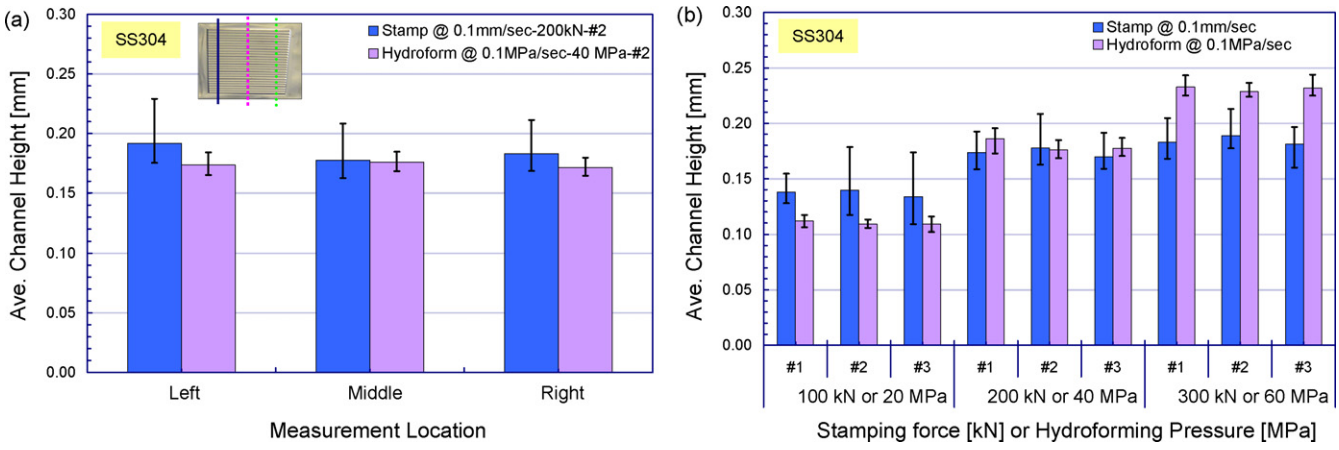

Fig. 6. Laser measurements showing (a) in-plate, and (b) between-plate variations.

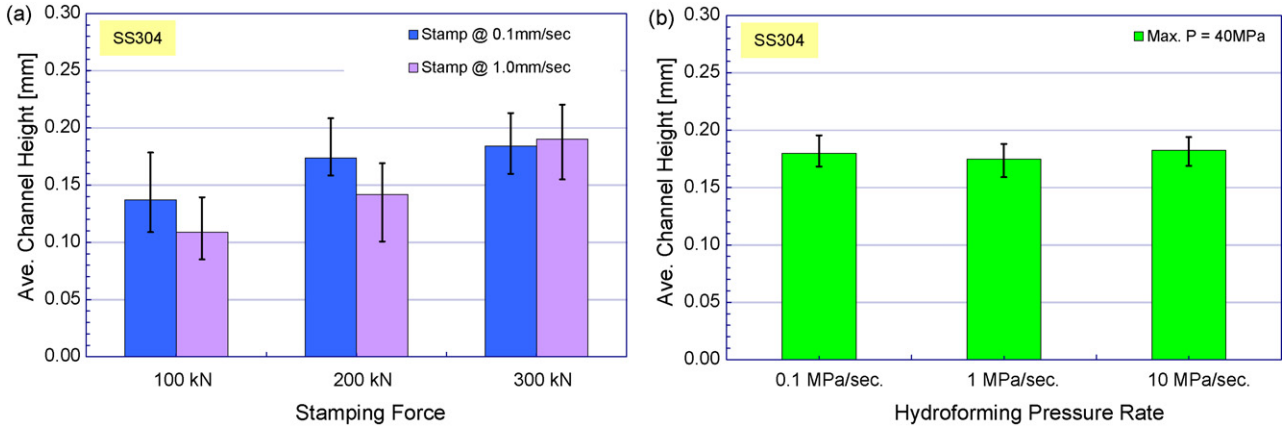

Fig. 7. Effect of (a) stamping speed, and (b) pressure rate on channel height.

hand, the between-plate variations (i.e., between three specimens formed under the same conditions) are shown in Fig. 6b. This value was found to be lower than 2.5% for stamping, and lower than 3.4% for hydroforming for all force and pressure levels used in this study. Note that for all cases, the hydroforming process yielded lower variations in terms of the channel height values among the 26 channels than stamping as shown by the max–min bar at the top of each bar graph.

3.2. Effect of process parameters on channel formability

The effect of the forming speed on the micro-channel formability is presented in Fig. 7. Two stamping speeds of 0.1 and 1 mm s^{-1} and three hydroforming pressure rates of 0.1, 1, and 10 MPa s^{-1} were selected with respect to the limitations and capabilities of the equipment and setup used in the experiments. Based on the measurement results, the stamping speed and force were shown to have negative and positive effects, respectively, on the channel height. That is lower channel height was obtained with increasing stamping speed or decreasing stamping force. Nevertheless, their interactive effect becomes diminished at a force level of 300 kN. In addition, the variation was found to be slightly worse with increasing stamping speed. On the other hand, for the hydroforming process, both the pressure and pressure rate were found to have significant effects on the channel formability based on a statistical analysis which yielded a P-value < 0.05, despite the slight difference in channel height values as observed in the histogram plots in Fig. 7b.

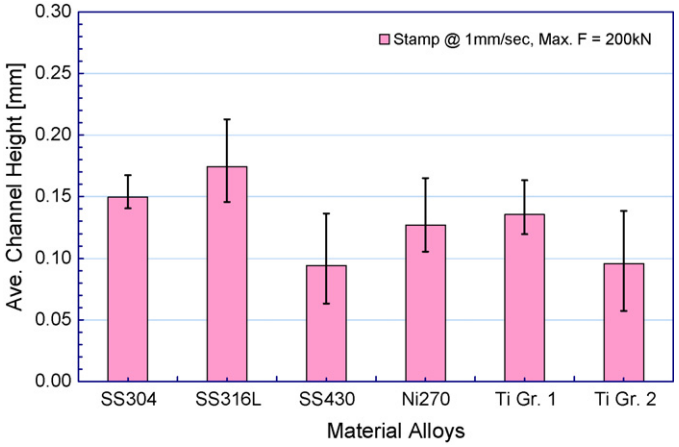

Fig. 8. Formability of different sheet alloys.

3.3. Effect of material type on channel formability

Several material candidates were investigated in terms of their formability limitation in the stamping process. Thin blanks of SS304, SS316L, SS430, Ni270, titanium grades 1 and 2 that have initial thickness of 0.051 mm were stamped at 200 kN force with a speed of 1 mm s^{-1}. The measured channel heights are shown in Fig. 8. Based on the results shown in Fig. 8, SS304 and SS316L demonstrated better formability when compared to other more expensive and stronger alloys as expected. For SS430 and titanium

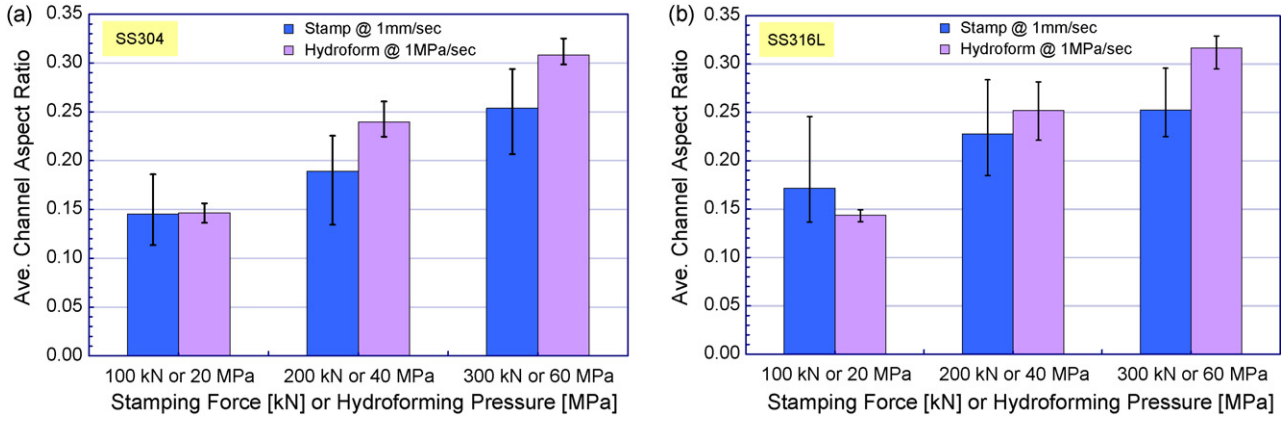

Fig. 9. Average channel aspect ratio as a function of forming force or pressure for (a) SS304, (b) SS316L.

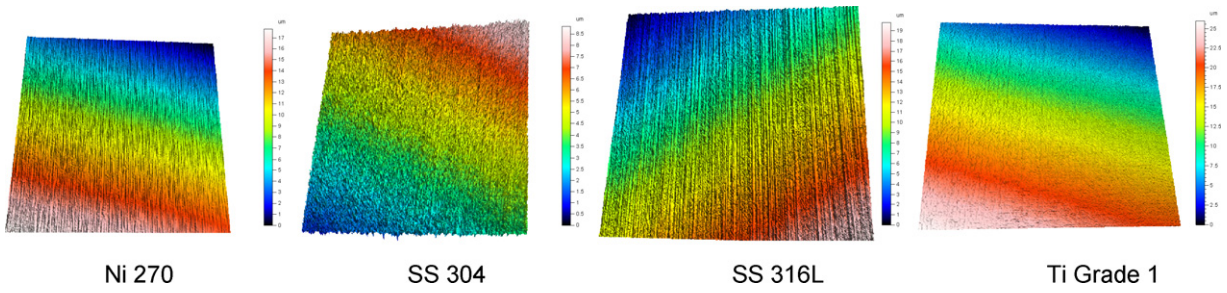

Fig. 10. Surface topographies of non-deformed blanks.

grade 2, some channel fractures were observed on the stamped specimens. It is, therefore, concluded that, cold stamping process may not be a suitable manufacturing process for these alloys. On the other hand, Ni270 and Ti grade 1 resulted in successful forming of the micro-channels with the maximum channel height value of around 0.13 mm. To determine the forming limit of these alloys, the force was increased from 200 kN to 400 kN, and if no fracture, to 600 kN. The results revealed some fractures on the Ni270 specimens at 400 kN, and on the Ti grade 1 specimens at 600 kN. Finally, it was observed that the materials with higher strength have larger variations in channel heights within the plate. Therefore, from the manufacturing point of view, SS304 and SS316L are promising, however, their corrosion resistance in their bare conditions is known to be not the best among the materials tested [11,14]. With appropriate coating, these two stainless steel alloys could become the material of choice for the economical and reliable PEMFC bipolar plates. To further compare the formability of SS304 and SS316L,

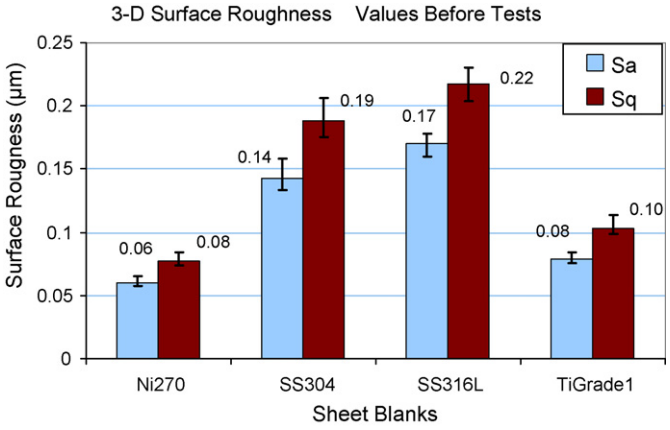

Fig. 11. 3D surface roughness values of non-deformed blanks.

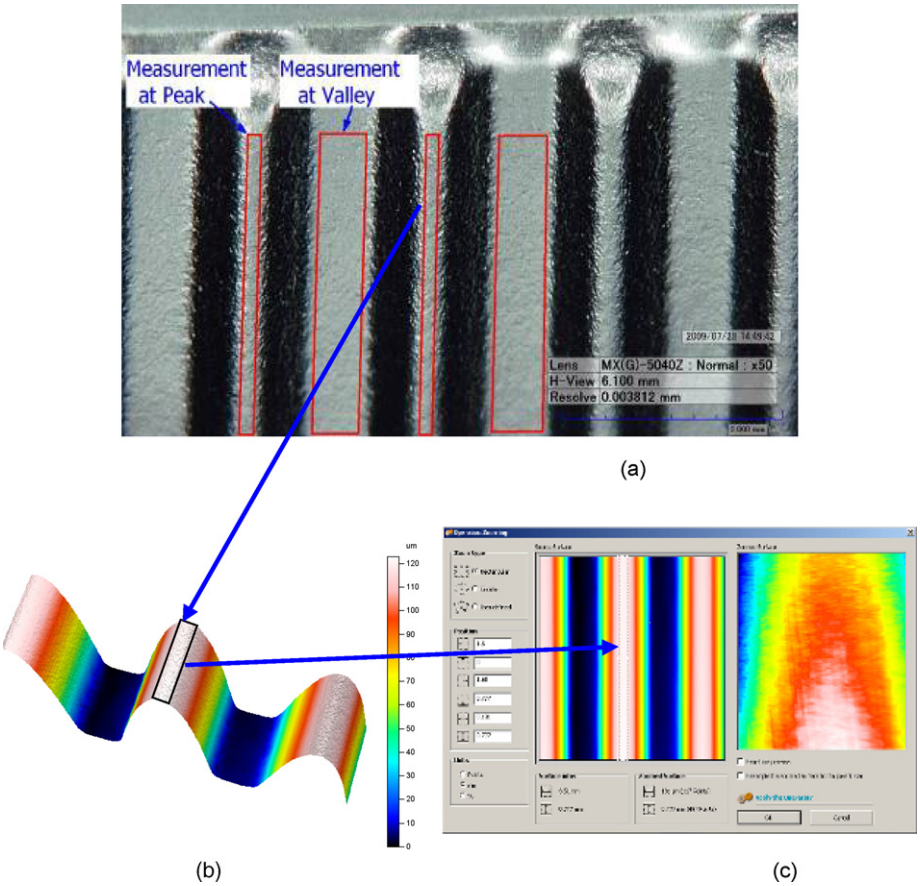

Fig. 12. (a) 3D surface roughness measurement locations (microscope picture with HIROX KH-7700, HIROX-USA, NJ, USA); (b) typical roughness measurement slit view in 3D; (c) boundary selection for the peak region measurement in µsoft analysis software. (Nanofocus AG,Oberhausen, Germany).

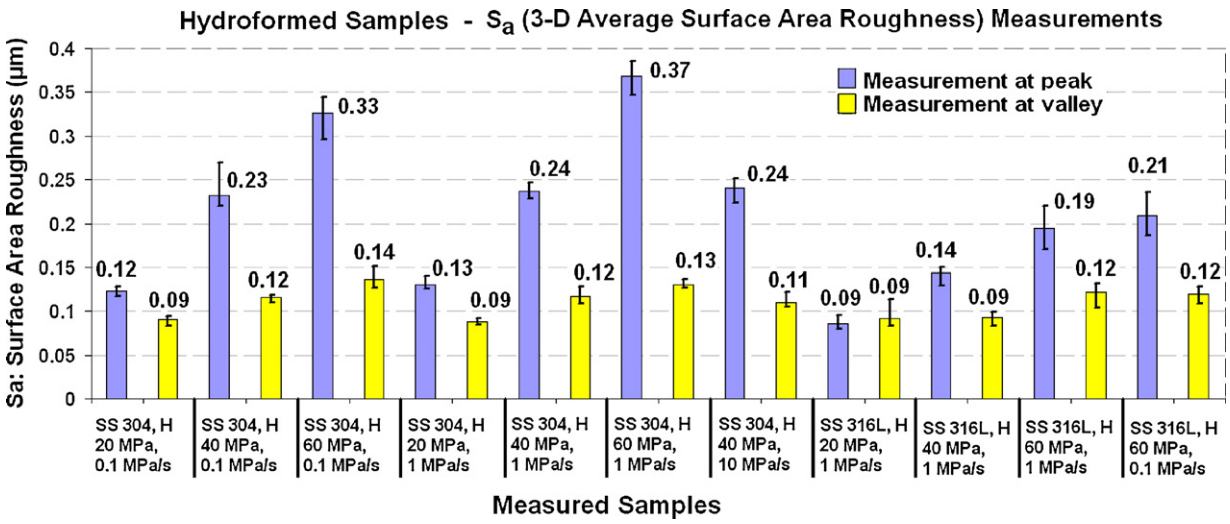

Fig. 13. 3D average surface area roughness (S_a) measurements for hydroformed samples.

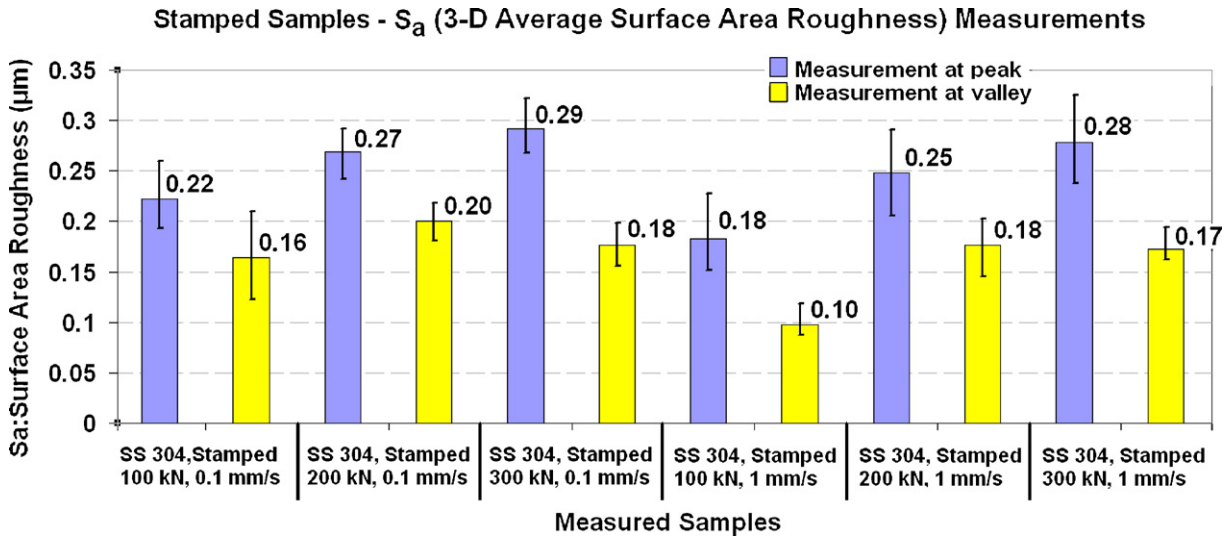

Fig. 14. 3D average surface area roughness (S_a) measurements for stamped samples.

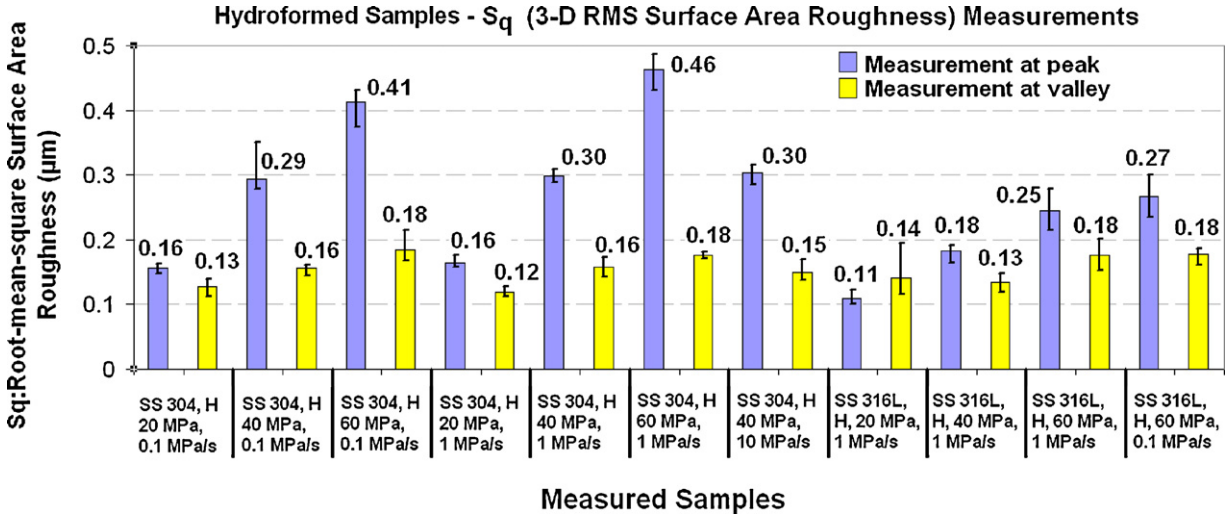

Fig. 15. 3D root-mean square roughness (S_q) measurements for hydroformed samples (violet bars are for peak, yellow bars are for valley measurements). (For interpretation of the references to color in this figure legend, the reader is referred to the web version of the article.)

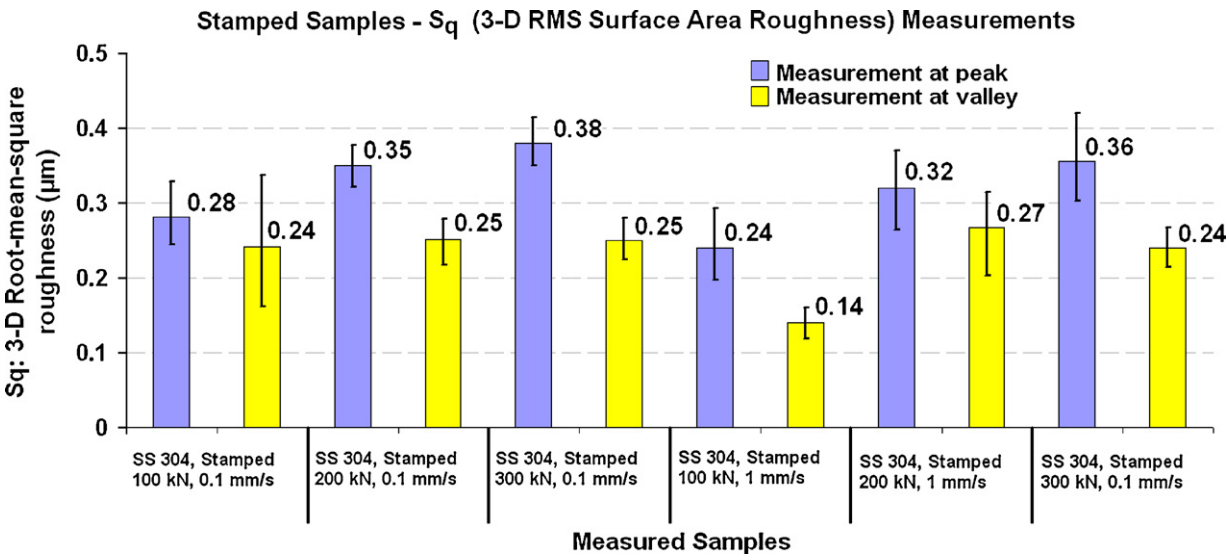

Fig. 16. 3D root-mean square roughness (S_q) measurements for stamped samples (violet bars are for peak, yellow bars are for valley measurements). (For interpretation of the references to color in this figure legend, the reader is referred to the web version of the article.)

both stamping and hydroforming processes were performed at different force and pressure levels (Fig. 9). The maximum aspect ratios were shown to be 0.25 and 0.30 by stamping and hydroforming, respectively, for both alloys. Therefore, the material formability of SS304 and SS316L is shown to be similar.

3.4. Effect of forming process on surface topography

Surface topography of the bipolar plates plays an important role on the corrosion and contact resistance of bipolar plates; and hence, on the performance and durability of the PEMFC stacks during actual working conditions. In general, bipolar plates with poor surface quality (i.e., rough surface) would lead to high contact resistance and low corrosion resistance. In this study, a confocal microscope capable of non-contact 3D-profiling (μsurf explorer, Nanofocus Inc., Glen Allen, VA, USA) was used to capture a 3D surface topography of the flat blanks and formed BPPs. In order to quantitatively compare the surface quality, several 3D surface roughness parameters, such as S_a (average surface area roughness), S_q (root-mean square roughness of the surface), were calculated and used in this study. These parameters provide the surface topography information spatially, as compared to the conventional 2D roughness measurement values (e.g., R_a and R_q). The surface topography and roughness values of flat blanks are shown in Figs. 10 and 11, respectively.

After the flat blanks were formed into an array of microchannels, surface roughness measurements were performed at the peak and valley locations as depicted in Fig. 12. In order to increase the reliability of the roughness measurements, at least three locations were measured on the same plate and used for calculating the average values as given in Figs. 13–16.

3.4.1. Effect of measurement locations (peak vs. valley)

The surface roughness measurements presented in Figs. 13–17 showed that higher surface roughness values were obtained at channel peaks than the in the valleys. Differences between the peak and valley measurements increase with the increasing hydroforming pressure and stamping force. The variations of the surface roughness values are the valleys were found to be lower than that at the channel peaks. It is noteworthy to mention that the valley locations were in direct contact with the die surface (Fig. 3), hence local deformation of asperities may have resulted in lower variations and surface roughness values. On the contrary, channel peaks were formed without die-blank direct contact. This effect can be seen as illustrated in Fig. 17 where the valleys had been smoothened, while channel sidewalls and peaks were shown to be roughened.

3.4.2. Effect of forming processes (stamping vs. hydroforming)

S_a measurements at the channel peaks in Figs. 13 and 14 showed that hydroformed plates have lower roughness value than the stamped plates when equivalent force/pressure levels are considered and compared (e.g., 20 MPa vs. 100 kN, and 40 MPa vs. 200 kN), except 60 MPa–300 kN comparison case. For instance, S_a value for the hydroformed plate under 20 MPa and 0.1 MPa s^{-1} condition was measured to be 0.12 while this value went up to 0.22 for the stamped plate under 100 kN, 0.1 mm s^{-1} conditions. The maximum roughness value among the hydroformed samples was measured to be 0.46 μm for SS304 blank formed at 60 MPa with 1 MPa s^{-1} pressure rate at the channel peaks. As for SS316L, the highest roughness value was found to be 0.27 μm at 60 MPa with 0.1 MPa s^{-1} pressure rate. Among the stamped samples, the highest surface roughness was found to be 0.38 μm on the specimen formed at 300 kN stamping force and 0.1 mm s^{-1} stamping speed. Similar behaviors were observed in S_q measurements as presented in Figs. 15 and 16.

On the other hand, hydroformed samples attained consistently lower surface roughness values than the ones for stamped sam-

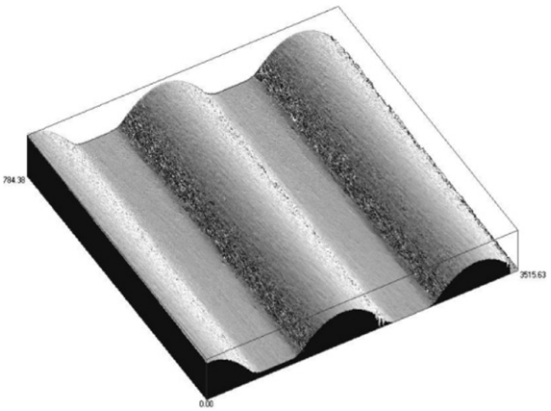

Fig. 17. Shaded surface texture image of formed channels.

ples at valley locations. For instance, S_q measurements acquired at the valleys varied between 0.12 μm and 0.18 μm for hydroformed samples, while the range was determined to be between 0.11 μm and 0.46 μm at the peaks.

3.4.3. Effect of forming force and pressure levels (kN, MPa)

It is clearly seen from Figs. 13–16 that the roughness values measured at channel peaks are proportional to both hydroforming pressure and stamping force. Furthermore, the effect of hydroforming pressure and stamping force on the surface roughness was found to be statistically significant ($P \leq 0.0003$ for both hydroforming, and stamping). However, the same conclusion is not valid for the measurements obtained at valleys, particularly for the stamped BPPs.

3.4.4. Effect of forming rates (mm s^{-1} and MPa s^{-1})

For hydroformed plates, higher pressure rates yielded higher surface roughness values at the channel peaks. In contrast, a faster stamping speed (1 mm s^{-1}) resulted in a smoother surface when compared to a slower speed (0.1 mm s^{-1}) at both measurement locations (peaks and valleys). The highest S_a value measured at the peaks was 0.37 μm under 60 MPa, 1 MPa s^{-1} hydroforming conditions, and as 0.29 μm under 300 kN and 0.1 mm s^{-1} stamping conditions. In other words, the surface roughness was found to be increased with increasing hydroforming pressure rate, but decreased with increasing stamping speed.

3.4.5. Effect of material types (SS304 vs. SS316L)

From materials point of view, relatively lower surface roughness values (S_a, S_q) values were observed on hydroformed SS316L plates when compared to SS304. As can be seen from Fig. 13, at 60 MPa and 1 MPa s^{-1} hydroforming conditions, surface roughness values for SS304 and SS316L samples were measured as 0.37 μm, and 0.19 μm, respectively.

3.4.6. Overall surface roughness evolution

In this analysis, surface roughness values for blanks are compared with the formed plates. When the valley location was considered, the hydroformed plates are smoother than the flat blanks for both SS304 (S_a: 0.14 μm) and SS316L (S_a: 0.17 μm) materials. When the peak location was considered, the surface roughness of hydroformed plates were found to be dictated by the level of the forming pressure. Specifically, for SS304, the surface roughness was improved at 20 MPa, but becomes rougher at higher pressure levels. Similarly, for SS316L the surface roughness was improved at 20 MPa and 40 MPa, regardless of the pressure rate, but becomes rougher at 60 MPa. Contrarily, for the stamped BPPs, the surface at the channel peaks was found to be rougher when compared to the flat blanks for both stainless steel materials.

4. Summary and conclusions

Stamping and hydroforming processes were shown to be viable solutions for mass production of micro-channel arrays on large thin plates to fabricate bipolar plates for PEMFC applications. The processes were shown to have low in-plate and between-plate variations with the maximum variation of less than 4.1% and 3.4% for stamping and hydroforming processes, respectively. However, hydroforming was observed to provide bipolar plates with lower dimensional variations than the stamping process. The effect of the stamping speed and force were shown to be significant, especially at low force levels, while their interaction effect was found to diminish at high force levels. Similarly, the effect of the pressure and pressure rate were found to be significant on the formability of the micro-channels. In terms of material type, SS304 and SS316L were observed to possess better formability when compared to other alloys tested in this study, while SS430 and Ti grade 2 showed the worst formability among all.

3D surface roughness measurements showed that the hydroformed bipolar plates generally yielded lower surface roughness values at the channel peaks when compared to stamped bipolar plates. When the roughness at peaks is compared with the ones obtained on the non-deformed blanks, it was found that up to a certain level of hydroforming pressure or stamping force, the surface roughness were improved. On the other hand, the valleys experienced surface smoothening as it was in a full contact with the die under a high hydrostatic load from the pressurized fluid. However, almost all stamped bipolar plates showed roughened surface topography when compared to flat blanks. Process speed was found to be another important factor on the surface quality. Higher stamping speeds and lower hydroforming pressure rates resulted in lower surface roughness values, regardless of the initial surface roughness values. SS316L samples attained lower roughness values in both S_a and S_q measurements when compared to SS304.

As a final remark, in a recent study by the authors, the effect of stamping and hydroforming process parameters on corrosion characteristics of the formed plates were investigated [8]. That study reported that the corrosion resistance decreases with decreasing stamping speed and increasing hydroforming pressure rate, corresponding to the results in this study where the surface roughness increases at a lower stamping speed and a higher pressure rate.

Acknowledgements

Authors are thankful to National Science Foundation (NSF) for the support on this project. It was supported by NSF I/UCRC Program (Center for Precision-CPF and its industrial members under NSF IIP Grant #: 0638588). The authors also would like to thank Hamilton Precision Metals, Inc. for supplying the sheet materials and their properties and to the CPF group members at VCU for their support during experiments. Surface topography analyses were obtained at Nanofocus-US (Glen Allen, VA) using μsurf explorer confocal microscope. Contributions of David Matthews, and Christian M. Wichern of Nanofocus-US are greatly acknowledged.

References

[1] S. Ream, Proceedings of the Fuel Cell Seminar, San Antonio, TX, 2007.
[2] J. Scherer, R. Stroebel, B. Gaugler, C. Schleier, R. Glueck, W. Berroth, Proceedings of the Fuel Cell Seminar, San Antonio, TX, 2007, pp. 166–169.
[3] F. Barbir, PEM Fuel Cells: Theory and Practice, Elsevier Academic Press, London, 2005.
[4] A. Hermann, T. Chaudhuri, P. Spagnol, International Journal of Hydrogen Energy 30 (2005) 1297–1302.
[5] X. Li, I. Sabir, International Journal of Hydrogen Energy 30 (2005) 359–371.
[6] M. Koç, S. Mahabunphachai, Journal of Power Sources 172 (2) (2007) 725–733.
[7] M. Tucker, G. Lau, C. Jaconson, L. Delonghe, S. Visco, Proceedings of the Fuel Cell Seminar, San Antonio, TX, 2007, p. 215.
[8] F. Dundar, E. Dur, S. Mahabunphachai, M. Koç, Journal of Power Sources 195 (2010) 3546–3552.
[9] H. Tawfik, Y. Hung, D. Mahajan, Journal of Power Sources 163 (2007) 755–767.
[10] A. Pozio, F. Zaza, A. Masci, R.F. Silva, Journal of Power Sources 179 (2008) 631–639.
[11] S. Wang, J. Peng, W. Lui, J. Zhang, Journal of Power Sources 162 (2006) 486–491.
[12] V.V. Nikam, R.G. Reddy, S.R. Collins, P.C. Williams, G.H. Schiroky, G.W. Henrich, Electrochimica Acta 53 (2008) 2743–2750.
[13] W. Yoon, X. Huang, P. Fazzino, K.L. Reifsnider, M.A. Akkaoui, Journal of Power Sources 179 (2008) 265–273.
[14] R.H.J. Blunk, D.J. Lisi, Y. Yoon, C.L. Tucker III, AIChE Journal 49 (1) (2003) 18–29.
[15] E. Middelman, W. Kout, B. Vogelaar, J. Lenssen, E. de Waal, Journal of Power Sources 118 (2003) 44–46.
[16] T.E. Lipman, J.L. Edwards, D.M. Kammen, Energy Policy 32 (2004) 101–125.
[17] T. Matsuura, M. Kato, M. Hori, Journal of Power Sources 161 (2006) 74–78.
[18] D. Liu, L. Peng, X. Lai, International Journal of Hydrogen Energy 34 (2009) 990–997.
[19] http://www.bac2.co.uk/images/FuelCellConstruction.jpg, Last access date: March 22, 2010.
[20] S. Mahabunphachai, M. Koç, Journal of Power Sources 175 (1) (2008) 363–371.